Title

Distinct Surface and Bulk Thermal Behaviors of LiNi0.6Mn0.2Co0.2O2 Cathode Materials as a Function of State of Charge

Journal

ACS Applied Materials & Interfaces, 12(10)

ISSN

1944-8244

Authors

Tian, Chixia

Xu, Yahong

Kan, Wang Hay

et al.

Publication Date

2020-03-11

DOI

10.1021/acsami.9b21288

Peer reviewed

Distinct Surface and Bulk Thermal Behaviors of $LiNi_{0.6}Mn_{0.2}Co_{0.2}O_2$ Cathode Materials as a Function of State-of-Charge

Chixia Tian,[a,b] Yahong Xu,[c] Wang Hay Kan,[d] Dimosthenis Sokaras,[c] Dennis Nordlund,[c] Hao Shen,[a,e] Kai Chen,[e] Yijin Liu,[c] and Marca Doeff.[a,*]

a) Energy Storage and Distributed Resources Division, Lawrence Berkeley National Laboratory, Berkeley, CA 94720

b) Academy of Integrated Science, Virginia Tech, Blacksburg, VA 24061, USA

c) Stanford Synchrotron Radiation Lightsource, SLAC National Accelerator Laboratory, Menlo Park, California 94025, USA.

d) Dongguan Neutron Science Center, Dongguan, Guangdong, 523803 China

e) Center for Advancing Materials Performance from the Nanoscale (CAMP-Nano), State Key Laboratory for Mechanical Behavior of Materials, Xi'an Jiaotong University, Xi'an, Shaanxi 710049, China

*Email: MMDoeff@lbl.gov

Keywords: lithium-ion battery, NMC-622 cathode, thermal behavior, X-ray absorption spectroscopy (XAS), X-ray Raman spectroscopy (XRS), Transmission X-ray microscopy (TXM)

Abstract

Understanding how the structural and chemical transformations take place in battery particles under thermal conditions can inform designing thermally robust electrode materials. Such a study necessitates the use of diagnostic techniques that are capable of probing the transformations at multiple length scales and at different states-of-charge (SOC). In this study, the thermal behavior of $LiNi_{0.6}Mn_{0.2}Co_{0.2}O_2$ (NMC-622) was examined as a function of SOC, using an array of bulk and surface sensitive techniques. In general, thermal stability decreases as lithium content is lowered, and conversion in the bulk to progressively reduced metal oxides (spinels, rock salt) occurs as the temperature is raised. Hard X-ray absorption spectroscopy (XAS) and X-ray Raman spectroscopy (XRS) experiments, which probe the bulk, reveal that Ni and Co are eventually reduced when partially delithiated samples (regardless the SOC) are heated, although Mn is not. Surface sensitive synchrotron techniques such as soft XAS and transmission X-ray microscopy (TXM), however, reveal that, for 50% delithiated samples, apparent oxidation of nickel occurs at particle surfaces under some circumstances. This is partially compensated by reduction of cobalt, but may also be a consequence of redistribution of lithium ions upon heating. TXM results indicate the movement of reduced nickel ions into particle interiors or oxidized nickel ions to the surface, or both. These experiments illustrate the complexity of the thermal behavior of NMC cathode materials. The study also informs the importance of investigating the surface and bulk difference as a function of SOC when studying the thermal behaviors of battery materials.

Introduction

Lithium-ion batteries (LIBs) have been credited for revolutionizing consumer electronics and electrical vehicles. Increasing the energy density and cycle life, reducing the cost and improving the safety have been continuing efforts to further advance the practical applications of LIBs.[1,2] The most successful commercial cathode materials in LIBs are based on layered transition metal oxides, where the charge compensation mostly takes place at the transition metal oxides.[3,4] However, the oxygen anions in the lattice also play an important role in battery performance. Most degradation pathways of layered oxides are associated with the chemical properties of oxygen anions.[5,6] Although the oxygen anions do not directly contribute to the reversible capacity, their orbital occupancies may change during electrochemical cycling because of the strong orbital hybridization with the transition metal d orbitals.[7–9] Several degradation processes in layered oxides can be directly attributed to the oxygen instability in the lattice, which include but do not limit to surface reconstruction caused by surface oxygen loss, and electrolyte oxidation caused by transfer of surface lattice oxygen to the electrolyte.[10–14] These degradation processes contribute to the failure of LIBs. For stoichiometric layered oxides, such as NMC materials ($LiNi_xMn_yCo_zO_2$; $x+y+z \approx 1$), the oxygen becomes less stable as the degree of delithiation gets higher.[10,15,16] The oxygen stability in the layered lattice is closely related to the thermal stability of these materials.

Details of the thermal behavior of metal oxide cathode materials for LIBs are of considerable interest, because of the potential for severe safety consequences associated with thermal runaway. As the Ni content in NMC cathodes is raised to improve practical energy densities, the thermal stability decreases.[17,18] Phase conversion to reduced metal oxides with concomitant oxygen release is known to occur upon heating of Ni-rich

cathode materials in high states-of-charge (SOC),[18–23] increasing the risk of fire in LIBs subjected to abuse. These phenomena are more complex than they at first appear; phase conversion is affected not only by temperature, but also time of exposure, and oxygen release is affected by sample heterogeneity,[24,25] particle size,[26] and morphology,[27] and also intimately connected to chemo-mechanical occurrences such as particle cracking.[28] Further complicating matters are interactions with other components in the cells such as carbon and binder.[29] To remove the effects of the latter, for this study, we prepared chemically delithiated $LiNi_{0.6}Mn_{0.2}Co_{0.2}O_2$ (NMC-622) samples to isolate reactions limited to those of the active materials themselves, and examined materials in several different SOCs, corresponding not only to overcharge conditions, but also normal top-of-charge (approximately 50% delithiated). We used several characterization methods designed to probe both particle surfaces and the bulk to understand the effects of thermal treatments on these model systems, with the goal of providing further information that might be useful for designing more robust cathode materials for safer batteries. This comprehensive characterization allowed us to discover that the NMC materials do not simply undergo continuous reduction upon thermal treatment as earlier studies have reported; instead the delithiated NMC particles show a large degree of variation from the surface to the bulk, which exhibits a strong dependence on the extent of delithiation. We anticipate that the insights based on the studies reported herein can lead to further improvements in cathode designs.

Experimental

Sample Preparation

Synthesis of solid spherical NMC-622 sample

Transition metal hydroxide ($TM(OH)_2$) precursor $Ni_{0.6}Mn_{0.2}Co_{0.2}(OH)_2$ was provided by a third party. Lithium hydroxide monohydrate (≥98.0%, Sigma Aldrich) was mixed with the $TM(OH)_2$ precursor in a molar ratio of 1.02:1 in an agate mortar for 20 mins. Then the mixture was transferred into a ball milling jar. Small amounts of acetone was added into the mixture to immerse the powder. Then the acetone and powder mixture was ball milled at low speed (200 rpm) for 60 min. and followed with milling at high speed (400 rpm) for another 60 min. The mixture was then dried under air to remove excess acetone. Then the dried product was annealed in a box furnace at 850 ^{o}C for 6 hrs under air flow with a 2 ^{o}C/min ramping rate for both heating and cooling steps.

Preparation of delithiated samples

All delithiated samples were prepared by chemical delithiation inside an argon-filled glove box. Briefly, a stock oxidant solution (i.e., 0.12M NO_2BF_4 in anhydrous acetonitrile) was prepared in advance to ensure that all the oxidant was well dissolved. Then NMC-622 powder was mixed with different amounts of the stock oxidant solution in the desired stoichiometric ratio to reach various delithiated states. For example, 0.3g (3.096E-3 moles) NMC-622 powder was added to 26 mL of 0.12M NO_2BF_4/acetonitrile solution and stirred in glovebox for 24 hrs to reach the "100%" delithiated state. All samples were then centrifuged and washed with pure acetonitrile three more times and dried under vacuum overnight. All the above procedures were done in an argon-filled glovebox (O_2 < 1 ppm and H_2O < 1 ppm).

Sample Characterization

Pristine and delithiated powder samples were dissolved in concentrated nitric acid and further diluted and analyzed with an inductively coupled plasma optical emission

spectrometer (ICP-OES, Perkin-Elmer Optima5400) to determine the chemical composition. Hot stage X-ray powder diffraction (XRD) studies were carried out using a Panalytical X'Pert Pro diffractometer equipped with an Anton Parr HTK 1200 hot stage using monochromatized Cu Kα radiation. The samples were heated in air at a ramping rate of 5 °C/min, then held for 15 min at the desired measurement temperature before data collection. The Le-Bail refinement was conducted in a GSAS-EXPGUI package.[32]

Synchrotron Characterization

For *ex situ* soft X-ray absorption spectroscopy (XAS) experiments, samples were mounted on an aluminum sample holder with double-sided carbon tape in an argon-filled glove box, transferred in a double-contained jar to a glove bag purged with argon connected to the XAS load-lock chamber. Measurements were conducted on the bending magnet beamline 8-2 at Stanford Synchrotron Radiation Lightsource (SSRL) using a ring current of 500 mA and a 1100 lines/mm spherical grating monochromator. The monochromator was operated with 40 μm entrance and exit slits, providing ~2.0×10^{10} ph s^{-1} at 0.4 eV resolution in a 0.1 × 0.1 mm^2 beam spot.[24] Data were acquired under ultrahigh vacuum (10^{-9} Torr) in a single load at room temperature using Auger electron yield (AEY, measured by a cylindrical mirror analyzer at constant kinetic energy), total electron yield (TEY, measured by sample drain current) and fluorescence yield (FY, measured with an IRD AXUV-100 silicon diode). All spectra were normalized by the incident current from a gold-evaporated fine grid positioned upstream of the main chamber. For transition metal L-edges, a linear fit background was removed and then the maximum intensities were normalized to unity.

Hard XAS measurements were carried out in both transmission and fluorescence modes at beamline 4-1 of SSRL. Calibration was applied to all spectra using the first inflection point of the corresponding Ni, Mn or Co metal foil. X-ray absorption near edge structure (XANES) data were analyzed using Athena software.[33]

3D full field transmission X-ray microscopy (FF-TXM) was performed at SSRL beamline 6-2c. Small amount of powder samples were loaded into quartz capillary tubes with diameters of 100 μm and wall thicknesses of 10 μm. Series of transmission images were collected as the energy of the incoming X-rays was scanned across the Ni absorption K-edge. The spatial resolution was ~30 nm. The energy step was set to be 1 eV in the near edge region and at a larger step size of 10 eV over the pre-edge and post edge regions, respectively. The energy window was set to a wide range for better normalization of the X-ray absorption spectra.[34] The initial data reduction was processed with an in-house developed software package TXM-Wizard,[35] and over 20 million XANES spectra were recovered with each one of them associated with a unique pixel in the image. The 0.5-intensity-cut of the K-edge was utilized to identify the relative oxidation states of transition metals.[61]

Ex situ X-ray Raman spectroscopy (XRS) measurements were performed at beamline 6-2b at SSRL. The samples were compressed into pellets and mounted onto the holder. The spectra were recorded with samples kept in helium atmosphere and each spectrum was a bandwidth of 1 eV. The X-ray Raman signals were collected with Si-660 reflection of the 40-crystal XRS spectrometer at 9694.8 eV with a monochromator Si (311) around 10.3 keV to have the Raman offset corresponding to Co L-edge, Ni L-edge and O K-edge.

Results and Discussion

In the present study, we chose to focus on chemical delithiation to produce oxidized samples because a cleaner surface for soft XAS analysis is needed, especially in the surface-sensitive electron yield mode. Figure 1a and 1b show XRD patterns of NMC-622 samples delithiated to various levels, prior to heating. Most of the samples retained the $R\bar{3}m$ structure after delithiation, with some shifting of peaks consistent with changes in the lattice parameters upon oxidation. An exception is the material that is nominally 100% delithiated. There is considerable peak broadening and a strong shift of the (003) reflection (lowest angle peak) rightward indicative of a marked decrease in the *c* lattice parameter. During the analogous electrochemical process, the H3 phase with a (003) reflection in Figure 1b, is observed only as a shoulder on the main low angle peak for this material when it is charged to an extremely high voltage (e.g., 5V).[15,36] However, for the chemical delithiation, the H3 phase exhibits a single symmetrical low angle peak with the decreased *c* lattice parameter. This implies that the lithium removal through chemical delithiation is complete. However, there is also a coalescence of the double peaks near $2\theta = 65°$ (Figure 1b) for the 100% delithiated sample, which suggests some loss of lamellarity and disordering at such high level of lithium removal. This may also be a consequence of a loss of crystallinity, as peak broadening is also evident. Proton insertion into layered cathodes has been reported in samples highly delithiated with NO_2BF_4,[37] which may have happened here. Apart from this sample, however, the bulk structural features of the chemically delithiated materials resemble those of the electrochemically oxidized analogs.[36,38,39]

Figure S1 details the results of *in situ* hot stage XRD experiments on the chemically delithiated materials with various lithium contents. There is a general trend to lower thermal stability with respect to phase conversion as lithium content decreases, as well as a tendency to form products containing progressively more reduced transition metal ions and lower oxygen contents. For the 10% delithiated NMC (Figure S1b), structural changes occur at and above about 300 °C, as evidenced by broadening of XRD peaks and a progressive decrease in the (003)/(104) peak intensity ratios, suggestive of some loss of lamellarity.[68] The results are consistent with formation of a "splayered" material; i.e., a layered material with some spinel character. The disordering is more evident at 300 °C for the 25% delithiated sample (Figure S1c), and above this temperature, changes in the patterns suggestive of partial formation of a separate spinel phase similar to $LiMn_2O_4$ occur.

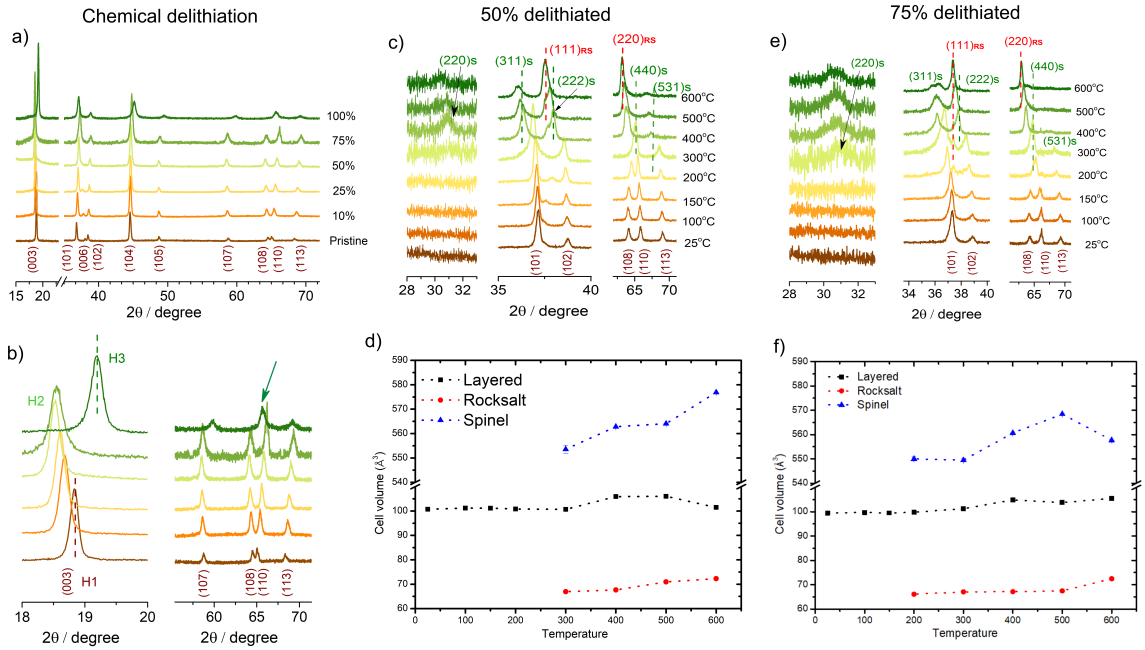

Figure 1. (a) XRD patterns of pristine and delithiated NMC-622 powders as a function of lithium content. (b) Expanded regions of (a) showing (003) reflections and peaks near 2θ

= 65°. Arrow points to the coalescence of the (108) and (110) peaks in the nominally 100% delithiated powder, which suggest a loss of lamellarity. (c) XRD patterns of the 50% delithiated powder as a function of temperature, and (d) cell volumes of phases produced upon heating taken from data in (c). (e) XRD patterns of the 75% delithiated powder as a function of temperature, and (f) cell volumes of phase produced upon heating taken from data in (e). The associated error analyses for Figures 1d and 1f are shown in Tables S1 and S2.

At 50% lithium content (Figure 1c and Figure S1d), disordering occurs at around 200 °C, and changes consistent with formation of disordered spinel occur above this temperature (e.g., coalescence of the double peaks near 2θ = 65°, and changes in relative intensities of reflections near 2θ = 35-40°). At 400 °C, the disordered spinel phase (resembling $LiMn_2O_4$) further changes to an M_3O_4-type spinel phase, implying a large loss of oxygen. The presence of the new phase is evidenced by a new set of peaks of the spinel phase as marked in Figure 1c (e.g., the (220) peak near 2θ = 31^o). In contrast, these changes occur at lower temperatures for the 75% delithiated NMC (Figures 1e and Figure S1e), with evidence of some M_3O_4 spinel present by 300 °C. Above this temperature, additional sharp peaks in the XRD patterns emerge (e.g., near 2θ = 37.5°), consistent with the presence of a rock salt phase, MO, which implies further loss of oxygen. For the fully delithiated sample, peak broadening in the XRD patterns is already observed at 150 °C (Figure S1f), and the sample is extremely disordered at 200 °C, although a sharp, weak peak near 2θ = 37.5°, tentatively belonging to rock salt or a mixture of rock salt and spinel is visible. Peaks become better defined at 300 °C and above and can be assigned to a mixture of rock salt and M_3O_4 spinel. These phenomena are consistent with the

observations in other thermally treated layered materials reported by Bak et al.[18] and Nam et al.,[20] even though different onset temperatures for the phase changes were reported because different compositions of materials were used in these reports.

We further confirmed the observed phase changes for NMC-622 with different lithium content by conducting Le Bail fitting for 50% and 75% delithiated samples that were treated at various temperatures. As shown in Figure 1d and Figure S2, layered, spinel and rock-salt phases coexist in the 50% delithiated sample at 300 ^{o}C. The corresponding unit cell volume changes are also shown in Figure 1d as a function of temperature. For the 75% delithiated NMC-622, these phase changes happen at a lower temperature (~200 ^{o}C) (Figure 1f and Figure S3).

The formation of spinel and MO-type phases for the more highly delithiated NMC-622 materials indicate that oxygen is lost during heating, an observation that has grave implications for battery safety. While *in situ* laboratory or synchrotron XRD experiments give vital information about the bulk behavior of cathode materials during heating, many details are lacking, such as how these phases propagate, their exact compositions, and the redox states of the metals (which is related to oxygen content) in some cases. Knowing these details may be helpful in guiding the design of more thermally robust materials and preventing catastrophic failure. To gain more insight on the thermal behavior, we investigated the structural and electronic properties of selected delithiated samples heated to either 170 °C or 350 °C in more detail as well as those of the pristine delithiated materials, using several different synchrotron X-ray techniques, to probe both surface and bulk changes. At 170 °C, most of the samples have not yet undergone major detectable phase conversions, while at 350 °C, loss of oxygen and

significant structural changes are well underway for the more highly delithiated materials. Thus, investigating materials heated to these two different temperatures give valuable information about the subtle changes that occur prior to major structural rearrangement as well as after.

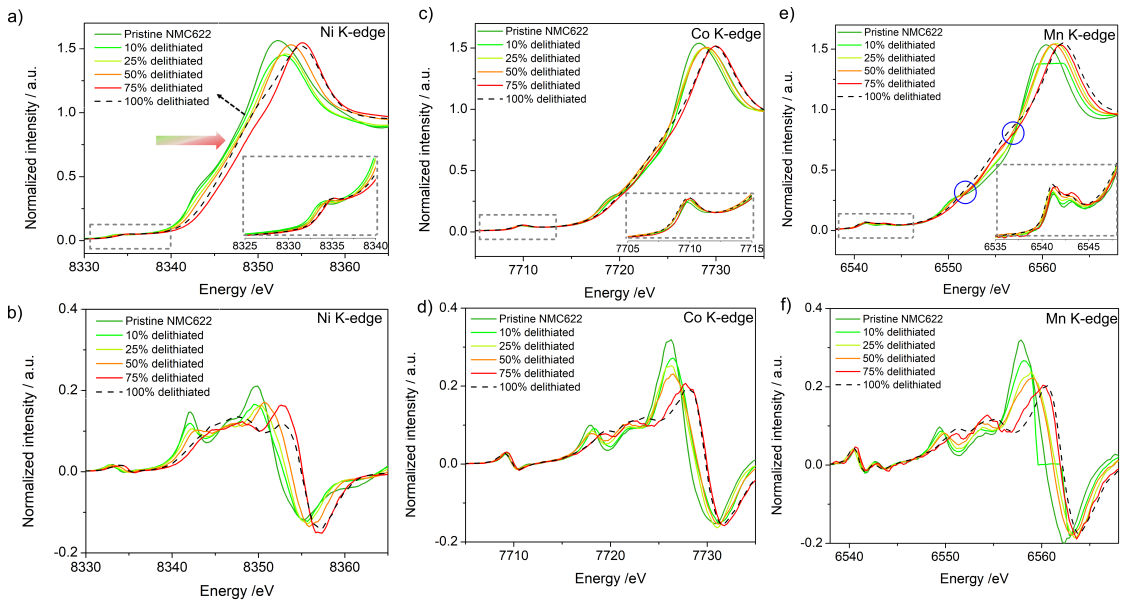

Figure 2. Hard XAS spectra of pristine and delithiated samples for (a) Ni K-edge, (c) Co K-edge, and (e) Mn K-edge. The inset figures show the pre-edge region. First derivative curves of these spectra for (b) Ni K-edge, (d) Co K-edge, and (f) Mn K-edge. The derivative curves are used here to display better visualization of peak (or energy) shifts of samples at different conditions.

Normalized XANES spectra for the Ni, Co, and Mn K-edges on the chemically delithiated samples are shown in Figures 2a, 2c, and 2e, respectively. In general, the XANES spectra can be divided into two regions: (1) the main absorption edge, which corresponds to transitions from the 1s to 4p states[40,41] and (2) the pre-edge peaks, which are usually ascribed to 1s to 3d transitions through a weak electric quadrupole transition. The transition probability of 1s to d orbital is less in comparison to the p orbital because

of orbital symmetry restrictions. However, the hybridization of d and p orbitals makes the electric dipole transition from 1s to the hybridized orbital (the p component rather than the d component) allowed and the pre-edge peak intensity become observable.[42,43] The shape of the XANES spectra gives information about the local geometry, while the absorption edge (i.e., the absorption edge determined based on the inflection point, or the energy where the intensity is 50% of the edge maximum, or the average of the energies at 20% and 80% of the edge maximum[40,44]) is sensitive to the oxidation states of the element of interest.[40–43]

In Figure 2a, there is a progressive shift of the Ni XANES spectra to higher energies (we use the energy where the intensity is 50% of the edge maximum as the indicator) as the lithium content decreases, consistent with charge compensation by oxidation of Ni in the bulk. An exception is the nominally 100% delithiated sample (black dashed curve in Figure 2a), for which, as previously discussed, proton insertion may have occurred. Another possible reason that the 100% delithiated sample has lower oxidation states than expected is that the sample loses its lamellarity as discussed in the previous XRD analysis. This causes the disassembly of the secondary and even primary particles through exfoliation and hence increases the surface area of the particles that can be exposed to the solvents and reactants during chemical delithiation. The surface reconstruction that normally happens at high state of charge may play a predominant role and becomes detectable even with bulk sensitive hard XAS. (The thermal behavior of this sample was not further studied herein because of its structural anomalies). Similar trends although with smaller changes are also observed in the pre-edge features (inset of Figure 2a). This is more clearly observable in the derivative plot (Figure 2b). Such changes have

been reported for $LiNi_{0.3}Mn_{0.3}Co_{0.3}O_2$ (NMC-333),[7,43] $LiNiO_2$[13] and $Li(Ni_{0.5}Co_{0.5})O_2$[45] materials, in which Ni is the only or dominant redox center upon charging and discharging.

The spectral changes for both Co and Mn upon delithiation are more complicated because no systematic edge shifting is observed. Instead, changes in the shapes of the edge features are observed, which can be related to the local coordination number, symmetry, and covalency with the coordinated ligands. For Co K-edge, it has been reported that the oxidation state of Co in NMC-333 material changes from 3+ to 4+ when the state of charge reaches more than 80%, where a cut-off voltage of 4.7 V is defined as 100% state of charge.[43] However, in another study, no such change was noticed even when NMC-333 was charged to 5V.[7] The ambiguity in interpretation of the K-edge data makes it difficult to conclude whether Co redox occurs for these samples, based on the subtle changes in the absorption edge and the pre-edge features (Figures 2b and 2e). Similarly, Mn K-edge spectra (Figures 2c and 2f) show shape changes but no systematic edge energy shifting. It is accepted that Mn remains tetravalent for NMC materials undergoing redox, when the spectra are compared with standard materials such as $Li_{1.2}Cr_{0.4}Mn_{0.4}O_2$[46], $LiNi_{0.5}Mn_{0.5}O_2$[47] and NMC-333.[7,43]

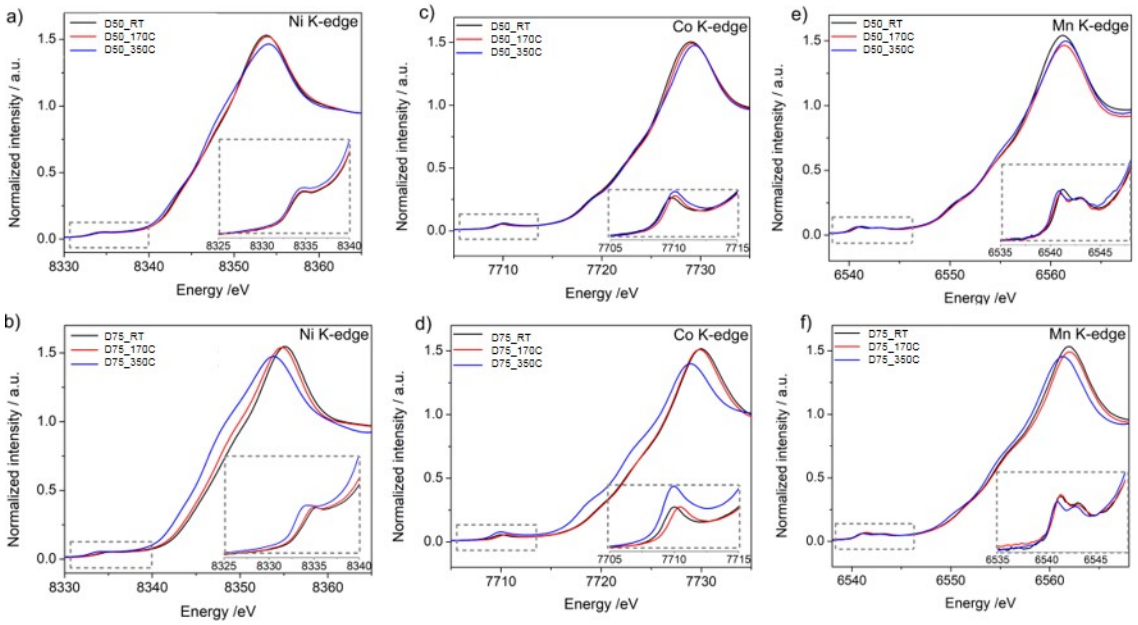

Figure 3. Ni K-edge, Co K-edge and Mn K-edge XANES spectra for (a, c, e) 50% and (b, d, f) 75% delithiated NMC-622 powders, at room temperature, and after heating to 170 °C or 350 °C. Inset figures show the pre-edge features of each sample and each element.

Figures 3a and 3b show *ex situ* Ni K-edge XANES results on the 50% and 75% delithiated materials heated to 170 °C or 350 °C, respectively. Negligible changes in the edge energies are observed for the 50% delithiated sample heated to 170°C for all of the transition metals (Figures 3a, 3c and 3e). At the higher temperature (i.e., 350 °C), a slight shift to lower energy is evident (more clearly seen in the derivative plot, Figure S4a) for the Ni K-edge (although not for the Mn or Co edges) indicating that Ni has been slightly reduced compared to the unheated material. At this temperature, conversion to a disordered $LiMn_2O_4$-like spinel is well underway (Figure 1c and d). The hard XAS results show evidence of metal reduction in the bulk at 350 °C, associated with the phase conversion. This implies that there is some loss of oxygen involved in formation of the $LiMn_2O_4$-type phase.

More pronounced systematic shifts to lower energies in the Ni and Co K-edge spectra (Figures 3b, 3d and S4b, S4d) occur for the 75% delithiated material, especially after it has been heated to 350 °C. This is consistent with the XRD results, which show the presence of an M_3O_4-type spinel and some rock salt at 300 °C. Formation of these phases require an average reduction of the valence states of the metal ions. Compared to Ni and Co, Mn exhibits almost no change at 170 °C for both samples with different lithium contents and for the 50% delithiated sample even up to 350 °C. There is a slight shift of Mn edge to lower energies at 350 °C for this sample (blue curve in Figures 3f and S4f), but it is marginal compared to the changes seen in the Ni and Co K-edges. This demonstrates the superior thermal stability of Mn and its critical role in the structural stabilization of the NMCs.

The insets of Figures 3a-3f are the pre-edge regions of the respective XANES spectra. As mentioned earlier, the pre-edge features are strongly influenced by the coordination number and coordination symmetry. Electric dipole transitions are allowed through p-d hybridization in tetrahedral symmetry, while only electric quadruple transitions (which are much less intense than dipole transitions) can occur in octahedral symmetry.[42,48] The relatively weak intensity of all the pre-edge peaks indicate that the transition metals are in octahedral symmetry rather than tetrahedral symmetry. A closer look at the pre-edge features reveals that Mn has two distinctly separated peaks (around 6541 and 6543 eV in the insets of Figures 3e and 3f), which indicates that Mn is in the tetravalent state as only one pre-edge peak is observed for trivalent Mn.[43,49] Thus, Mn remains 4+ throughout the heating procedures for both 50% and 75% delithiated samples. This is consistent with our previous conclusion that was based on the main absorption

edge energy analysis. Two pre-edge peaks have been reported for $LiCoO_2$[44] and NMC-333[43] materials, where they attributed the two peaks to 1s to t_{2g} and 1s to e_g transitions. However, the splitting of pre-edge peaks for Co is not so well structured in some other reports for NMC and lithium nickel cobalt aluminum oxide ($LiNi_{0.8}Co_{0.15}Al_{0.05}O_2$, NCA) materials[7,20] as well as in our case. Regardless, the pre-edge peak intensity change contains more information. As shown in the insets of Figure 3c and 3d, the pre-edge peak intensity remains almost unchanged for the 50% delithiated sample heated to 350 °C, while there is a significant increase of peak intensity for the 75% delithiated sample after heating to 350 °C. The increasing intensity indicates the symmetry distortion around Co site.[20] This can be explained by the fact that Co migrates to the adjacent tetrahedral site in the highly delithiated sample heated to high temperatures to form the spinel phase, as observed in the XRD analysis. In contrast, the Ni pre-edge peak intensity (insets in Figures 3a and 3b) did not change, indicating that it did not migrate to tetrahedral sites due to the thermal abuse. However, there is a peak shift to lower energies (same as the main edge) for the 75% delithiated sample heated to 350 °C. To briefly summarize the XANES data, both Ni and Co undergo reduction in the highly delithiated materials heated to high temperatures, while Mn remains its tetravalent state. In addition, Co migrates to tetrahedral sites, resulting in a phase change from a layered structure to spinel.

The hard XAS results are broadly consistent with the *in situ* hot stage XRD findings. Both experiments characterize the bulk behavior, but the soft XAS data (Figure 4) paint a more complex picture of what happens during heating, especially at the surface. Soft XAS experiments probe surface to near-surface areas of samples, with the depth being examined dependent upon the detector in use. At the Stanford Synchrotron

Radiation Lightsource, we employed three types of detectors: Auger electron yield (AEY, probing 1-2 nm into the surface), total electron yield (TEY, about 5 nm in), and fluorescence yield (FY mode, 50-100 nm in). The spot size of ~1 mm means that many thousands of particles are examined simultaneously in a powdery sample, so that the results are ensemble-averaged.

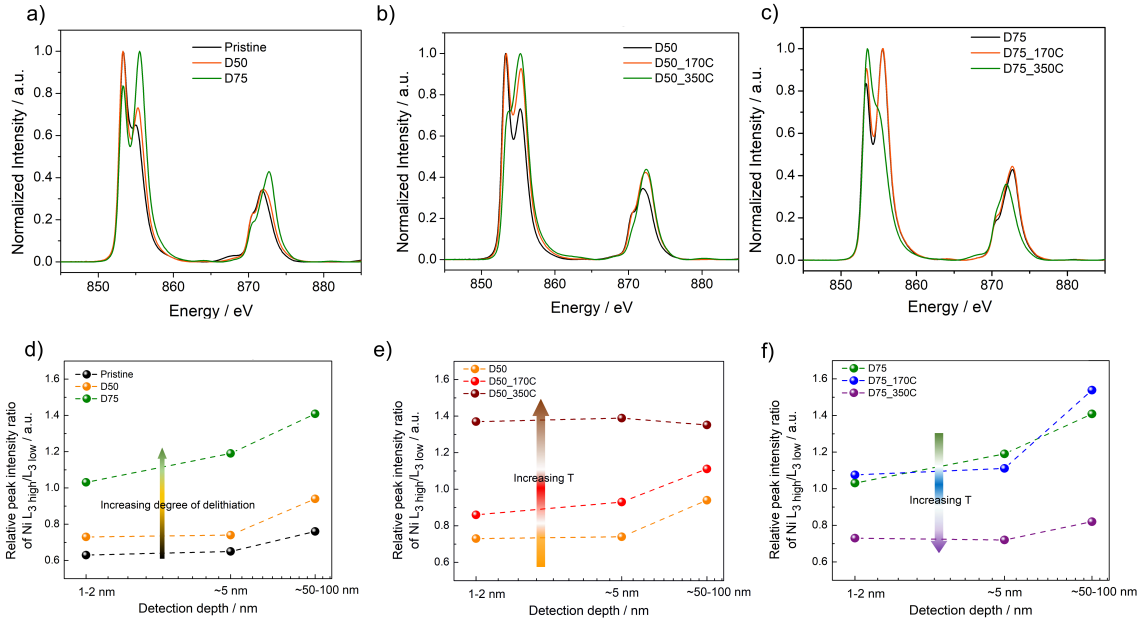

Figure 4. Ni L-edge XAS data in TEY mode for (a) pristine, 50%, and 75% delithiated powders, (b) 50% delithiated powders at room temperature and after heating to 170 °C or 350 °C, and (c) 75% delithiated powders at room temperature and after heating to 170 °C or 350 °C. The L_3 edge (centered at 855 eV) is split into two peaks; we use L_{3high} and L_{3low} to represent the peaks centered at higher and lower energies, respectively. Ni L_{3high}/L_{3low} ratios at different probing depths (AEY, 1-2 nm, TEY, 5 nm, and FY, 50-100 nm) for (d) pristine, 50%, and 75% delithiated powders, (e) 50% delithiated powders at room temperature and after heating to 170 °C or 350 °C, and (f) 75% delithiated powders at room temperature and after heating to 170 °C or 350 °C.

Figures 4a-c show the Ni L-edge TEY results for pristine, 50% and 75% delithiated samples before and after heating to 170 °C or 350 °C. The spectra show characteristic L_3 doublet peaks near 853 eV corresponding to the $2p_{3/2} \rightarrow 3d$ transition and a L_2 peak ($2p_{1/2} \rightarrow 3d$) near 870 eV. The ratios of the intensities of the L_{3high} to L_{3low} peaks give qualitative information about the Ni redox states, with higher values indicating a greater degree of oxidation.[15,50,51] The changes in the relative peak intensities can be clearly observed in Figure 4a for the pristine material and the delithiated samples, which indicate that the Ni oxidation state increases as the lithium content decreases. Figure 4d shows the values of L_{3high}/L_{3low} for the AEY, TEY, and FY data on these materials; i.e., the relative Ni oxidation states as a function of probing depth. For the as-made material, prior to delithiation, the average oxidation state of Ni is slightly lower near the surface than farther into the bulk. The oxidation state gradient also exists for the two partially delithiated materials. The gradient is symptomatic of surface reconstruction from a layered structure to a rock salt phase.[10,52] Surface reconstruction is a commonly observed phenomenon for NMC electrodes, and occurs under a variety of conditions, although it tends to be more pronounced after electrochemical charge than for chemical delithiation.[50]

Figure 4e summarizes the results for the 50% delithiated material before and after heating to 170 °C or 350 °C. The average oxidation state of Ni rose after the 170 °C treatment, although it was still lower near the surface than deeper into the sample. A marked increase in average Ni oxidation state occurred after heating to 350 °C, with homogenization throughout the top 50-100 nm of the sample. A comparison to the Ni K-edge data, however, indicates significant differences between the surface and the bulk

deeper than 100 nm in, the latter of which shows evidence of Ni reduction after heating to 350 °C rather than oxidation. The behavior of the 75% delithiated sample is markedly different from that of the 50% delithiated material (Figure 4f). A slight intensification of the Ni oxidation state gradient is observed after heating to 170 °C, but otherwise there is little change on average. In contrast, a dramatic reduction in the average Ni oxidation state after heating to 350 °C occurred at all depths that were probed as was found with the Ni K-edge data (i.e., in the bulk). Our results indicate that what occurs at or near the surface is drastically different from the bulk behavior and it is also closely related to the extent of delithiation (i.e., the state of charge).

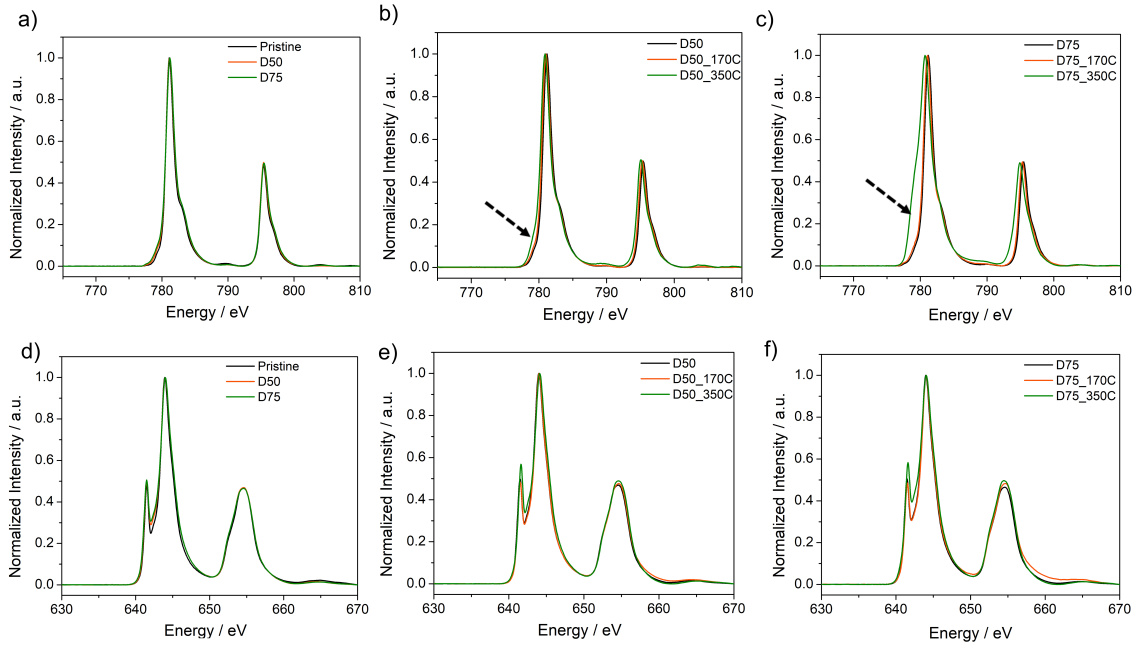

Figure 5. (a, b, c) Co L-edge XAS data and (d, e, f) Mn L-edge XAS data for (a, d) pristine, 50% and 75% delithiated powders, (b, e) 50% delithiated powders at room temperature and after heating to 170 °C or 350 °C, and (c, f) 75% delithiated powders at room temperature and after heating to 170 °C or 350 °C.

Figures 5a-c and 5d-f show the Co L-edge TEY and Mn L-edge TEY data, respectively, for the pristine, delithiated, and heated samples. Here, little change is seen in Co and Mn oxidation states as a function of lithium content (Figures 5a and 5d), at least at ~5 nm deep into the sample (TEY mode). This is similar to what was found in the K-edge data, which showed only modest changes in the average oxidation state for Co, and no change for Mn. Very slight broadening and peak shifting of the Co L_3 peak at about 783 eV (Figure 5b, for the 50% delithiated material) to the lower energy side after heating to 170 °C and a more significant broadening and shifting after the 350 °C treatment indicate that Co is reduced,[53] but little change is observed in the Mn L-edge data (Figure 5e). Thus, the surface oxidation of Ni that was observed for this sample is at least partly compensated for by the reduction of Co. For the 75% delithiated sample (Figures 5c and f), more significant peak broadening and shifting to lower energy occurs at the Co L_3 edge, particularly after heating to 350 °C, evidence for greater reduction of Co than in the 50% delithiated sample. Little change is observed in the Mn L-edge spectra (Figure 5f). This again is consistent with the bulk results, where Mn exhibits superior thermal stability.

Figure 6 shows the O K-edge spectra for the samples under investigation, in TEY mode. The integrated intensity of these peaks is proportional to the concentration of O hole states, and increases as the samples become more oxidized (Figure 6b). In other words, charge compensation upon oxidation is borne at least partly by oxygen and reflects the degree of covalency of the TM-O bonds. Our previous study included a detailed picture of the TM-O peak positions for standard transition metal oxides and can be found in reference 15 and is also plotted in Figure 6a. In this paper, we calibrated the

peak position of Li_2CO_3 to 534 eV (brown curve in Figure 6a). Figure 6b shows the pristine and delithiated samples before heat treatment. The sharp feature at 534 eV in the pristine (as-made) material can be attributed to π^*(C=O) in Li_2CO_3, a commonly observed impurity in Ni-rich NMCs, stemming from the synthesis conditions.[15] This peak is not observed in the O K-edge TEY data for the two partially delithiated samples, indicating that the chemical oxidation and washing process resulted in removal of Li_2CO_3, similar to what occurs during electrochemical oxidation[15]. The set of peaks between about 528 and 534 eV belong to lattice oxygen coordinated to various transition metals (TM-O). The use of the standards aids in assigning peaks in the pristine NMC-622 where Mn is tetravalent, Co is trivalent and Ni is intermediate between +2 and +3. The sharp peak centered around 529 eV belongs to Ni^{3+}-O (compare to the $LiNiO_2$ standard, blue curve in Figure 6a and blue dashed line indicated in Figure 6b) and the increase in intensity of this peak further confirms that Ni is oxidized during delithiation.

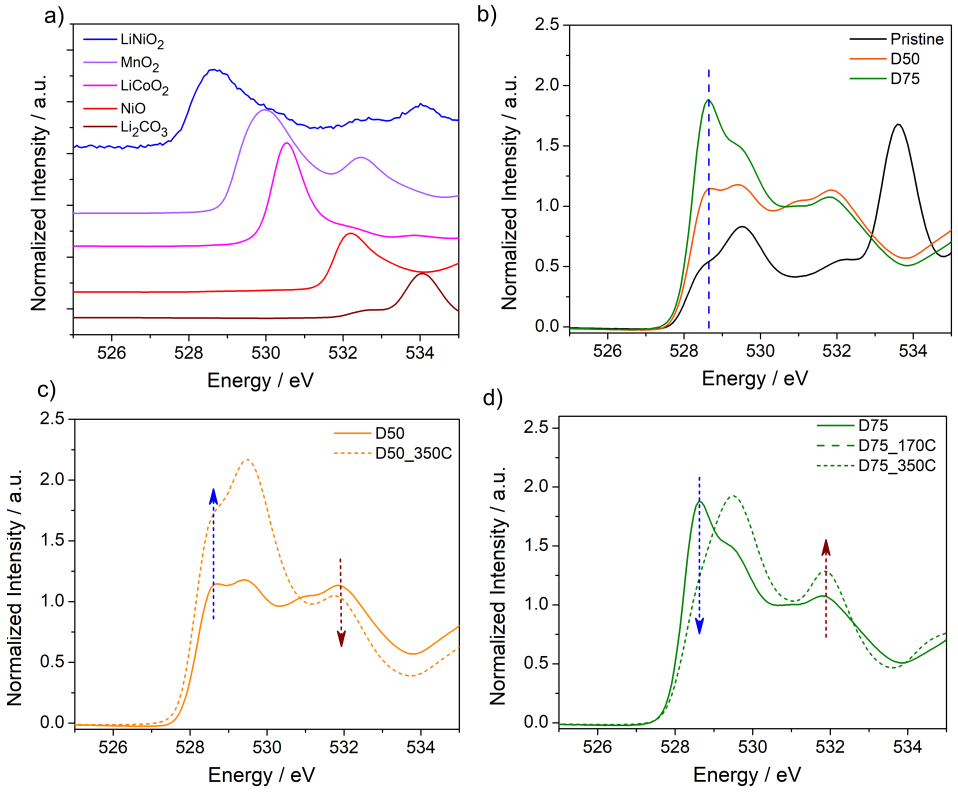

Figure 6. O K-edge data in TEY mode for: (a) different standards including $LiNiO_2$, MnO_2, $LiCoO_2$, NiO and Li_2CO_3. The same set of standards were used and taken from reference [15], (b) pristine, 50% and 75% delithiated powders, (c) 50% delithiated powders at room temperature and after heating to 350 °C, and (d) 75% delithiated powders at room temperature and after heating to 350 °C. All measurements were conducted ex-situ and at room temperature.

Figures 6c and d show that the lattice oxygen peaks change in intensity for both the 50% and 75% delithiated powders after heating to 350 °C. The blue dashed arrows (around 529 eV) indicate the peak associated with Ni^{3+}-O, while the brown dashed arrows (around 532 eV) mark Ni^{2+}-O and some contribution from the Mn^{4+}-O. It is clear that the Ni^{3+}-O peak of the 50% delithiated sample increased in intensity after heating, indicating oxidation of Ni at the surface. For the 75% delithiated sample, the peak around

529 eV diminished after heating to 350 °C, while the peak intensity related to Ni^{2+}-O increased. These results are consistent with the Ni L-edge results (Figures 4b and 4c) and further confirm that, upon heating to 350 °C, Ni is oxidized at the surface of the 50% delithiated sample while it is reduced at the 75% delithiated sample surface. Highly delithiated NMC materials are prone to lose oxygen, leading to a lower valence state of Ni and formation of NiO-like rock salt structure by reacting with electrolyte[10,15,54–56] or through thermal treatment.[18,20,21,28,57] Therefore, it is somewhat surprising to observe that Ni is oxidized at the surface upon heating in the 50% delithiated sample.

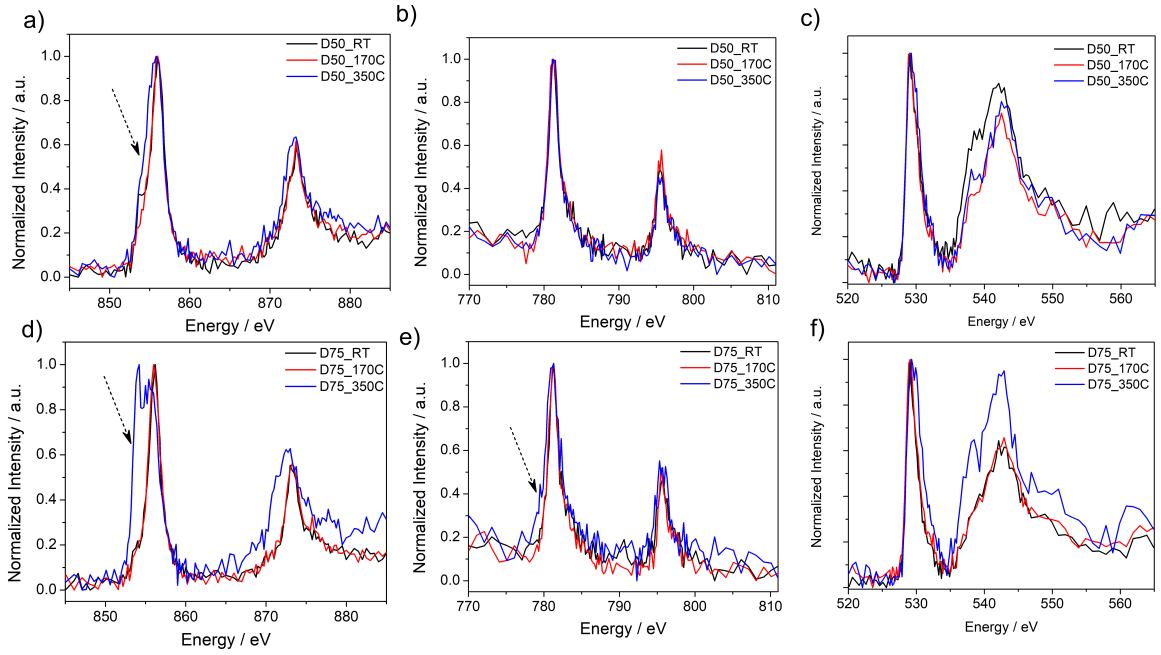

Figure 7. X-ray Raman data: (a, d) Ni L-edge, (b, e) Co L-edge, and (c, f) O K-edge for (a, b, c) 50% delithiated and (d, e, f) 75% delithiated powders at room temperature and after heating to 170 °C or 350 °C. Arrows point to regions of significant peak shifting and broadening for several of the samples.

Figure 7 shows *ex situ* X-ray Raman spectroscopy (XRS) data for the 50% and 75% delithiated powders before and after heating to 170 °C or 350 °C. XRS, provides a

means for extracting the information content of soft X-ray spectra while maintaining the bulk sensitivity benefits of hard X-ray techniques, allowing information to be obtained on the transition metals and oxygen behavior deeper into the sample.[58] Because it is a hard x-ray photon-in/photon-out technique, it offers the advantages of a hard x-ray probe while providing the sensitivity of soft XAS.[59] This can be seen by comparing the data in Figure 7a, where obvious broadening of the Ni L_3 edge near 855 eV to a lower energy is observed for the 50% delithiated powder heated to 350 °C, to that of the Ni K-edge XANES in Figure 2c, where there is very little change observed. The separation of L3 peaks observed in the soft XAS results are not as evident in the XRS spectra due to the limited energy resolution of XRS, however, the basic features are the same. As with soft XAS, shifting of the Ni L_3-edge to lower energy implies reduction of Ni in the bulk for both the 50% and 75% delithiated samples after heating to 350 °C. This difference is much more obvious for the 75% delithiated NMC-622 (Figure 7d). Similarly, broadening to lower energies of the Co peak for the 75% delithiated material heated to 350 °C (Figure 7e), indicative of reduction, is consistent with the changes observed in the Co K-edge XANES spectra (Figure 3). It is clear from Figure 7b that the average Co oxidation state is unaffected by heating the 50% delithiated NMC-622 to either temperature, and also that heating to 170°C has little effect on either the average Ni or the Co oxidation state in the bulk for either sample.

XANES is somewhat limited in the ability to probe light elements such as C, N and O, hence XRS serves as an alternative to the conventional hard XAS techniques in investigating systems with light elements.[58] The oxygen K-edge Raman data is shown in Figures 7 c and f for the 50% and 75% delithiated NMC-622 samples, respectively. The

peak near 530 eV corresponds to TM-O hybridization. It is clear that there is very little change upon heating for the 50% delithiated NMC-622, indicating that oxidation occurs only on the surface (based on the soft XAS data). For the 75% delithiated material heated to 350 °C, there is peak broadening. In this case, the shift to higher energy suggests the decrease of the hole states in the O2p orbitals. However, with a complicated system like NMC, where all three transition metals contribute to the TM-O hybridization peak, caution should be used in interpreting this shift simply as reduction of the transition metal. The formation of new phases with different degrees of TM-O covalency also alters the peak positions and intensity. However, it can be surmised that the surface oxidation that was detected with soft XAS for the 50% delithiated sample upon heating does not extend into the bulk.

It is curious that, in some cases (e.g., in the 50% delithiated sample) metals on surfaces are oxidized after heating although they are reduced in the bulk overall. To further investigate this, we employed TXM to probe both 50% and 100% delithiated particles before and after heating to 350 °C. The 100% delithiated sample was used as a test case, because the more severe reduction offers better visualization. The soft XAS spectra of Ni, Mn, Co L-edges and O K-edge (probing the surface), and the Ni XANES results (probing the bulk) of the 100% delithiated sample are presented in Figure S5 and S6 and indicate that the surface and bulk behaviors show similar trends to that of the 75% delithiated sample, although Ni reduction is more significant.

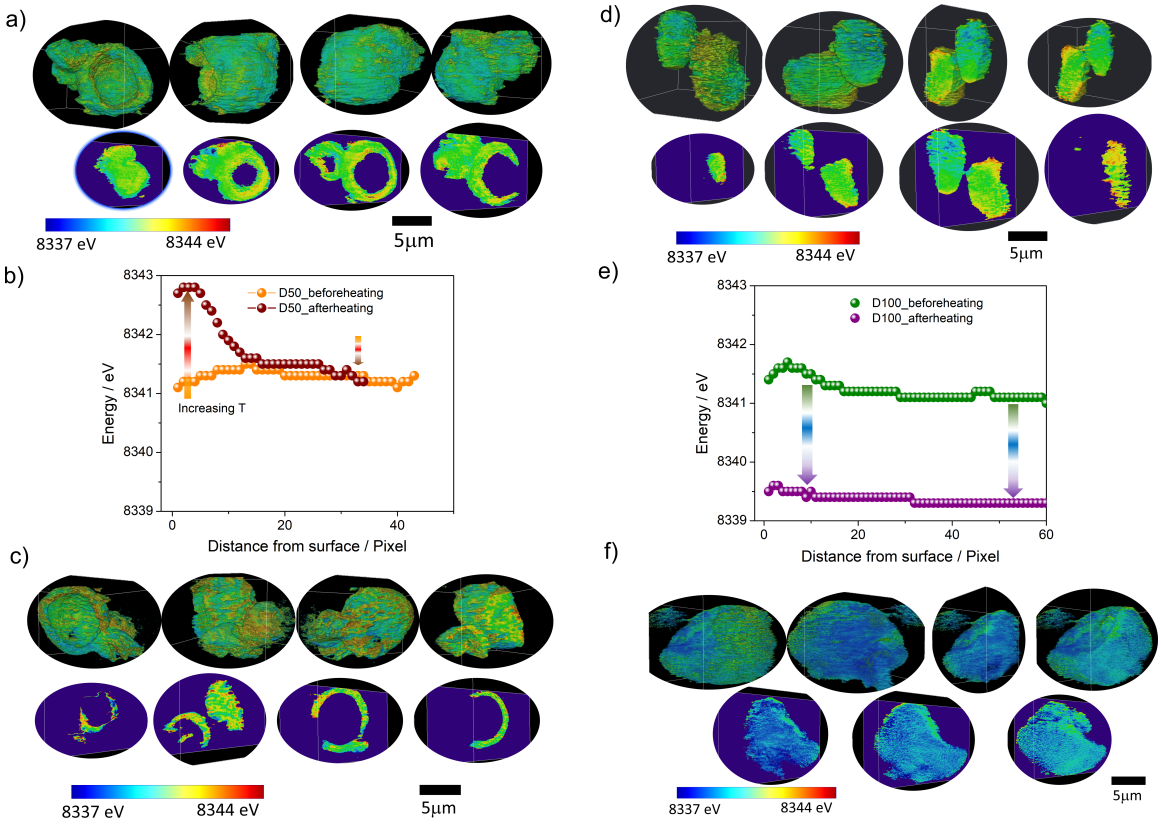

Figure 8. TXM images of a (a, c) 50% delithiated and (d, f) 100% delithiated NMC-622 particle before (a, d) and after (c, f) heating to 350 °C. Ni K-edge energies are color-mapped with blue representing lower oxidation states and red representing higher oxidation states. Ni K-edge energy was plotted as a function of distance from the particle surface before and after the (b) 50% delithiated particle and (e) 100% delithiated particle are heated.

The Ni K-edge energies are color mapped for a single particle of the 50% delithiated sample (Figures 8a and c) and the 100% delithiated sample (Figures 8d and f) before and after heating to 350 ^{o}C. Higher energies (red color end) indicate a higher average oxidation state. In Figures 8a, c, d and f, the top row images in each panel are 3D reconstructed views of particles from different angles and the bottom row images are sliced views (2D) of the particles. Comparing Figures 8a and 8c, it is clear that the

surfaces have been oxidized for the 50% delithiated sample (denser red spots on the surface of the particle) after heating to 350 ^{o}C. In contrast, the Ni in the 100% delithiated particle is significantly reduced as indicated by the blue color throughout the particle (Figures 8d and 8f). However, all views show that there is considerable heterogeneity in the distribution of Ni oxidation states. Heterogeneity has also been reported for different types of cathode materials (e.g., $LiFeO_4$, $LiCoO_2$, NMC, $LiNi_{0.5}Mn_{0.5}O_2$) that undergo electrochemical cycling, chemical or thermal treatment.[22,28,50,57,60–65] heterogeneity can be attributed to the intrinsic properties of the materials (e.g., particle size, shape, surface facets, conductivity), the electrical and/or ionic wiring, the chemomechanical propagation, and ion diffusivity or migration under different external stimulation.[66,67]

To eliminate the effects of the heterogeneous distribution on the data analysis and to quantify the depth of Ni oxidation phenomenon upon heating for the 50% delithiated sample, the energies (i.e., Ni oxidation states) are plotted as a function of distance from the surface in Figure 8b for the unheated and heated particle. Although the average Ni oxidation state increases slightly from the surface into the bulk for the unheated particle (consistent with the soft XAS data shown in Figure 4), the Ni valence appears to be relatively homogeneous throughout the depth. In contrast, there is a steep Ni oxidation state gradient for the particle after it has been heated, with a higher Ni oxidation state, on average, at the surface than in the interior. Since each pixel has a spatial resolution about 30 nm, the oxidation occurs roughly to a depth of ~350 nm and with the top 100 nm being significantly more oxidized (the probing depth of soft XAS FY mode). In the case of the 100% delithiated sample, there is a uniform reduction of Ni throughout the particle (Figure 8e).

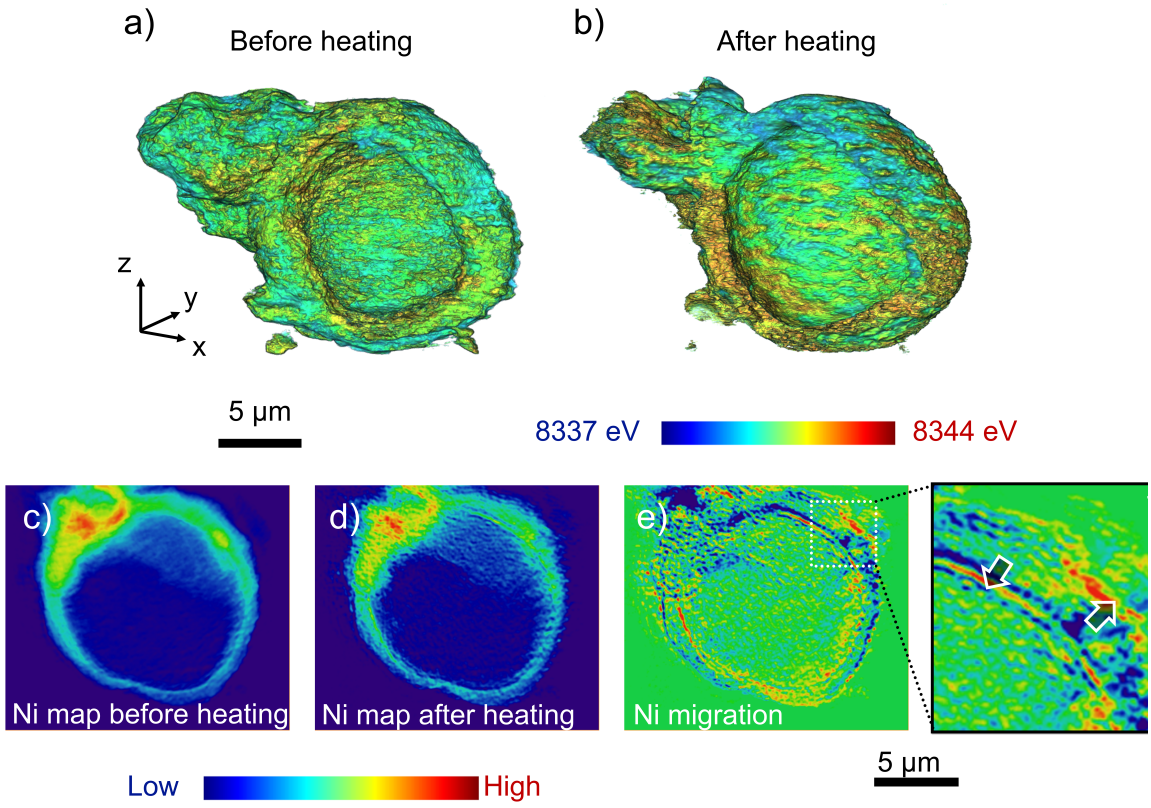

Figure 9. A closer look at the TXM images of the 50% delithiated NMC-622 particle (a) before and (b) after heating to 350 °C. Ni K-edge energies are color-mapped with red representing a higher valence state and blue representing a lower valence state. Ni content distributions in the particle (c) before and (d) after heating. The red corresponds to higher Ni content and blue lower Ni content. A map of Ni migration (differences between the locations of Ni before and after heating the particle) is shown in (e) with the area in the white box expanded in (f). Arrows point to areas where Ni has concentrated upon heating, and the Ni enrichment is found in both the exterior and interior surface regions of the hollow NMC622 particle.

Figure 9 shows more detailed TXM results on a 50% delithiated NMC-622 particle before and after heating to 350 ^{o}C. The results provide some additional information that can possibly explain the oxidation behavior on the surface upon heating.

The images showing Ni distributions throughout the 50% delithiated particle before (Figure 9c) and after (Figure 9d) heating give some insights into what may have happened. It is clear from these images that the Ni distribution has changed throughout the particle after heating. The difference map in Figure 9e quantifies this, with the expanded area to the right of the figure showing a region with particularly notable differences. The apparent oxidation state gradient that is observed in the heated particle may reflect the migration of lower valent Ni into the interior (or the migration of higher valent Ni to the surface) as reactions occur. However, the difference could also be attributed to the slight deformation of the particle upon heating. A recent study has shown that thermally-driven redistribution of Li ions can possibly lead to the charge transfer behavior between the bulk oxygen anions and the surface transition metal cations for lithium and manganese rich layered cathode materials.[65] Therefore, it is also likely that lithium ions migrate during the heating process, with local changes in transition metal oxidation states for the 50% delithiated sample, which does not involve Ni migration. Further studies regarding the unambiguously underlying mechanism of such distinct surface and bulk redox behaviors and the exact extent of delithiation (i.e., somewhere between 50% and 75% delithiation) that such surface behavior converts are underway. The study justifies the importance of combing surface and bulk sensitive, spatially resolved characterization techniques to reveal the disparate and complicated surface and bulk thermal behaviors of NMC materials as a function of SOC. It is also noted that understanding the transition metal transport properties during thermal events is important for several different cathode materials, including previously reported Li rich cathodes.[69]

Conclusions

The present study aims to unravel how the multiscale chemical and structural characteristics of NMC-622 materials transform during thermal conditions. We thoroughly investigated the bulk-to-surface transformations of NMC-622 materials at different states of charge. The complex thermal behavior of NMC-622 cathode materials, delithiated to differing SOCs, was revealed by a comprehensive study of bulk and surface properties of samples after heating. Bulk conversion to spinel and rock salt phases occurs, with lower transition temperatures occurring for materials with lower lithium contents. Several of these phase transitions involve oxygen evolution and transition metal reduction, the latter of which was confirmed for Ni and Co by hard XAS and XRS measurements. Mn, in contrast, remains tetravalent for the samples and temperatures that were studied. Soft XAS measurements showed that the surface behavior was considerably different than in the bulk, however, with higher Ni oxidation states observed on particle surfaces for the heated 50% delithiated NMC-622. Using TXM, a Ni oxidation state gradient was also observed for this sample after heating to 350 °C, with the surface to a depth of about 350 nm in more oxidized than the bulk. Mapping of the Ni content before and after heating to this temperature revealed that a redistribution of the metal occurs, which provides a possible explanation for the apparent paradoxical result. The present study represents one of the most comprehensive spectroscopic, scattering, and imaging studies for the thermal properties of NMC cathode materials to date. The comprehensive characterization allowed us to discover that the materials do not simply undergo continuous reduction as most studies have reported; instead the delithiated NMC particles show a large degree of variation from the surface to the bulk, which exhibits a strong dependence on the extent of delithiation. We also found that there was likely metal

segregation at the mesoscale based on the TXM results. Therefore, these results collectively imply that inhibiting the metal segregation would be an important path towards improving the thermal stability of Ni-rich layered cathodes.

Acknowledgments

This work was supported by the Assistant Secretary for Energy Efficiency and Renewable Energy, Office of Vehicle Technologies of the U.S. Department of Energy under Contract No. DE-AC02-05CH11231. The synchrotron X-ray portions of this research were carried out at the Stanford Synchrotron Radiation Lightsource, a Directorate of SLAC National Accelerator Laboratory and an Office of Science User Facility operated for the U.S. Department of Energy Office of Science by Stanford University. Use of the Stanford Synchrotron Radiation Lightsource, SLAC National Accelerator Laboratory, is supported by the U.S. Department of Energy, Office of Science, Office of Basic Energy Sciences under Contract No. DE-AC02-76SF00515. W.H.K. thanks the support from the National Natural Science Foundation of China (11805034 and 21704105), and Natural Science Foundation of Guangdong Province, 2017A030313021.

infringe privately owned rights. Reference herein to any specific commercial product, process, or service by its trade name, trademark, manufacturer, or otherwise, does not necessarily constitute or imply its endorsement, recommendation, or favoring by the United States Government or any agency thereof, or the Regents of the University of California. The views and opinions of authors expressed herein do not necessarily state or reflect those of the United States Government or any agency thereof or the Regents of the University of California.

Supporting Information

The Supporting Information is available free of charge on the ACS Publications website. XRD patterns and refinements, derivative analysis of hard XAS, soft and hard XAS.

Author contribution

C.T. designed and performed the experiments. M.M.D. supervised the project. Y.X. and Y.L. performed TXM experiments and data analysis. W.H.K assisted the XRD analysis. D.S. and D.N. participated in the XRS and XAS measurements. H.S. assisted the XRS experiments. K.C. participated in the scientific discussion. C.T. and M.M.D. analyzed the data and wrote the paper with assistance from all coauthors.

Note

The authors declare no competing financial interest.

References

(1) Evarts, E. C. Lithium Batteries: To the Limits of Lithium. *Nature* **2015**, *526* (7575), S93–S95.

(2) Goodenough, J. B.; Park, K.-S. The Li-Ion Rechargeable Battery: A Perspective. *J. Am. Chem. Soc.* **2013**, *135* (4), 1167–1176.

(3) Xu, B.; Qian, D.; Wang, Z.; Meng, Y. S. Recent Progress in Cathode Materials Research for Advanced Lithium Ion Batteries. *Mater. Sci. Eng. R Reports* **2012**, *73* (5), 51–65.

(4) Fergus, J. W. Recent Developments in Cathode Materials for Lithium Ion Batteries. *Journal of Power Sources*. **2010**, pp 939–954.

(5) Yoon, W. S.; Kim, K. B.; Kim, M. G.; Lee, M. K.; Shin, H. J.; Lee, J. M.; Lee, J. S.; Yo, C. H. Oxygen Contribution on Li-Ion Intercalation-Deintercalation in $LiCoO_2$ Investigated by O K-Edge and Co L-Edge X-Ray Absorption Spectroscopy. *J. Phys. Chem. B* **2002**, *106* (10), 2526–2532.

(6) Chen, C. H.; Hwang, B. J.; Chen, C. Y.; Hu, S. K.; Chen, J. M.; Sheu, H. S.; Lee, J. F. Soft X-Ray Absorption Spectroscopy Studies on the Chemically Delithiated Commercial $LiCoO_2$ Cathode Material. *J. Power Sources* **2007**, *174* (2), 938–943.

(7) Yoon, W. S.; Balasubramanian, M.; Chung, K. Y.; Yang, X. Q.; McBreen, J.; Grey, C. P.; Fischer, D. A. Investigation of the Charge Compensation Mechanism on the Electrochemically Li-Ion Deintercalated $Li1\text{-}XCo_{1/3}Ni_{1/3}Mn_{1/3}O_2$ Electrode System by Combination of Soft and Hard X-Ray Absorption Spectroscopy. *J. Am. Chem. Soc.* **2005**, *127* (49), 17479–17487.

(8) Yoon, W.-S.; Chung, K. Y.; McBreen, J.; Fischer, D. A.; Yang, X.-Q. Electronic Structural Changes of the Electrochemically Li-Ion Deintercalated $LiNi_{0.8}Co_{0.15}Al_{0.05}O_2$ Cathode Material Investigated by X-Ray Absorption Spectroscopy. *J. Power Sources* **2007**, *174* (2), 1015–1020.

(9) Kim, M. G.; Shin, H. J.; Kim, J.-H.; Park, S.-H.; Sun, Y.-K. XAS Investigation of Inhomogeneous Metal-Oxygen Bond Covalency in Bulk and Surface for Charge Compensation in Li-Ion Battery Cathode $Li[Ni_{1/3}Co_{1/3}Mn_{1/3}]O_2$ Material. *J. Electrochem. Soc.* **2005**, *152* (7), A1320.

(10) Lin, F.; Markus, I. M.; Nordlund, D.; Weng, T.-C.; Asta, M. D.; Xin, H. L.; Doeff, M. M. Surface Reconstruction and Chemical Evolution of Stoichiometric Layered Cathode Materials for Lithium-Ion Batteries. *Nat. Commun.* **2014**, *5*, 3529.

(11) Tornheim, A.; Sharifi-Asl, S.; Garcia, J. C.; Bareño, J.; Iddir, H.; Shahbazian-Yassar, R.; Zhang, Z. Effect of Electrolyte Composition on Rock Salt Surface Degradation in NMC Cathodes during High-Voltage Potentiostatic Holds. *Nano Energy* **2019**, *55*, 216–225.

(12) Xu, J.; Lin, F.; Nordlund, D.; Crumlin, E. J.; Wang, F.; Bai, J.; Doeff, M. M.; Tong, W. Elucidation of the Surface Characteristics and Electrochemistry of High-Performance $LiNiO_2$. *Chem. Commun.* **2016**, *52* (22), 4239–4242.

(13) Xu, J.; Hu, E.; Nordlund, D.; Mehta, A.; Ehrlich, S. N.; Yang, X.-Q.; Tong, W. Understanding the Degradation Mechanism of Lithium Nickel Oxide Cathodes for Li-Ion Batteries. *ACS Appl. Mater. Interfaces* **2016**, *8* (46), 31677–31683.

(14) Jung, S.-K.; Gwon, H.; Hong, J.; Park, K.-Y.; Seo, D.-H.; Kim, H.; Hyun, J.; Yang, W.; Kang, K. Understanding the Degradation Mechanisms of

$LiNi_{0.5}Co_{0.2}Mn_{0.3}O_2$ Cathode Material in Lithium Ion Batteries. *Adv. Energy Mater.* **2014**, *4* (1), 1300787.

(15) Tian, C.; Nordlund, D.; Xin, H. L.; Xu, Y.; Liu, Y.; Sokaras, D.; Lin, F.; Doeff, M. M. Depth-Dependent Redox Behavior of $LiNi_{0.6}Mn_{0.2}Co_{0.2}O_2$. *J. Electrochem. Soc.* **2018**, *165* (3), A696–A704.

(16) Li, J.; Downie, L. E.; Ma, L.; Qiu, W.; Dahn, J. R. Study of the Failure Mechanisms of $LiNi_{0.8}Mn_{0.1}Co_{0.1}O_2$ Cathode Material for Lithium Ion Batteries. *J. Electrochem. Soc.* **2015**, *162* (7), 1401–1408.

(17) Noh, H.-J.; Youn, S.; Yoon, C. S.; Sun, Y.-K. Comparison of the Structural and Electrochemical Properties of Layered $Li[Ni_xCo_yMn_z]O_2$ (x = 1/3, 0.5, 0.6, 0.7, 0.8 and 0.85) Cathode Material for Lithium-Ion Batteries. *J. Power Sources* **2013**, *233*, 121–130.

(18) Bak, S.-M.; Hu, E.; Zhou, Y.; Yu, X.; Senanayake, S. D.; Cho, S.-J.; Kim, K.-B.; Chung, K. Y.; Yang, X.-Q.; Nam, K.-W. Structural Changes and Thermal Stability of Charged $LiNi_xMn_yCo_zO_2$ Cathode Materials Studied by Combined In Situ Time-Resolved XRD and Mass Spectroscopy. *ACS Appl. Mater. Interfaces* **2014**, *6* (24), 22594–22601.

(19) Wu, L.; Nam, K. W.; Wang, X.; Zhou, Y.; Zheng, J. C.; Yang, X. Q.; Zhu, Y. Structural Origin of Overcharge-Induced Thermal Instability of Ni-Containing Layered-Cathodes for High-Energy-Density Lithium Batteries. *Chem. Mater.* **2011**, *23* (17), 3953–3960.

(20) Nam, K. W.; Bak, S. M.; Hu, E.; Yu, X.; Zhou, Y.; Wang, X.; Wu, L.; Zhu, Y.; Chung, K. Y.; Yang, X. Q. Combining in Situ Synchrotron X-Ray Diffraction and

Absorption Techniques with Transmission Electron Microscopy to Study the Origin of Thermal Instability in Overcharged Cathode Materials for Lithium-Ion Batteries. *Adv. Funct. Mater.* **2013**, *23* (8), 1047–1063.

(21) Hwang, S.; Kim, S. M.; Bak, S. M.; Kim, S. Y.; Cho, B. W.; Chung, K. Y.; Lee, J. Y.; Stach, E. A.; Chang, W. Using Real-Time Electron Microscopy To Explore the Effects of Transition-Metal Composition on the Local Thermal Stability in Charged $Li_xNi_yMn_zCo_{1-y-z}O_2$ Cathode Materials. *Chem. Mater.* **2015**, *27* (11), 3927–3935.

(22) Gent, W. E.; Li, Y.; Ahn, S.; Lim, J.; Liu, Y.; Wise, A. M.; Gopal, C. B.; Mueller, D. N.; Davis, R.; Weker, J. N.; Park, J.-H.; Doo, S.-K.; Chueh, W. C. Persistent State-of-Charge Heterogeneity in Relaxed, Partially Charged $Li_{1-x}Ni_{1/3}Co_{1/3}Mn_{1/3}O_2$ Secondary Particles. *Adv. Mater.* **2016**, *28* (31), 6631–6638.

(23) Bak, S. M.; Nam, K. W.; Chang, W.; Yu, X.; Hu, E.; Hwang, S.; Stach, E. A.; Kim, K. B.; Chung, K. Y.; Yang, X. Q. Correlating Structural Changes and Gas Evolution during the Thermal Decomposition of Charged $Li_xNi_{0.8}Co_{0.15}Al_{0.05}O_2$ Cathode Materials. *Chem. Mater.* **2013**, *25* (3), 337–351.

(24) Tian, C.; Xu, Y.; Nordlund, D.; Lin, F.; Liu, J.; Sun, Z.; Liu, Y.; Doeff, M. Charge Heterogeneity and Surface Chemistry in Polycrystalline Cathode Materials. *Joule* **2018**, *2*, 1–14.

(25) Hu, E.; Wang, X.; Yu, X.; Yang, X. Q. Probing the Complexities of Structural Changes in Layered Oxide Cathode Materials for Li-Ion Batteries during Fast Charge-Discharge Cycling and Heating. *Acc. Chem. Res.* **2018**, *51* (2), 290–298.

(26) Judith Alvarado, Chenxi Wei, Dennis Nordlund, Thomas Kroll, Dimosthenis Sokaras, Yangchao Tian, Yijin Liu, M. M. D. Thermal Stress-Induced Charge and Structure Heterogeneity in Emerging Cathode Materials. *submitted*.

(27) Wei, C.; Zhang, Y.; Lee, S.-J.; Mu, L.; Liu, J.; Wang, C.; Yang, Y.; Doeff, M.; Pianetta, P.; Nordlund, D.; Du, X.-W.; Tian, Y.; Zhao, K.; Lee, J.-S.; Lin, F.; Liu, Y. Thermally Driven Mesoscale Chemomechanical Interplay in $Li_{0.5}Ni_{0.6}Mn_{0.2}Co_{0.2}O_2$ Cathode Materials. *J. Mater. Chem. A* **2018**, *6* (45), 23055–23061.

(28) Mu, L.; Lin, R.; Xu, R.; Han, L.; Xia, S.; Sokaras, D.; Steiner, J. D.; Weng, T. C.; Nordlund, D.; Doeff, M. M.; Liu, Y.; Zhao, K.; Xin, H. L.; Lin, F. Oxygen Release Induced Chemomechanical Breakdown of Layered Cathode Materials. *Nano Lett.* **2018**, *18* (5), 3241–3249.

(29) Wang Qingsong; Ping Pinga; Zhao Xuejuan; Chu Guanquan; Sun Jinhua; Chen Chunhua. Thermal Runaway Caused Fire and Explosion of Lithium Ion Battery. *J. Power Sources* **2012**, *208*, 210–224.

(30) Kim, J. Y.; Kim, S. H.; Kim, D. H.; Susanto, D.; Kim, S. Y.; Chang, W. Y.; Cho, B. W.; Yoon, W. S.; Bak, S. M.; Yang, X. Q.; Nam, K. W.; Chung, K. Y. Electronic Structural Studies on the Improved Thermal Stability of $Li(Ni_{0.8}Co_{0.15}Al_{0.05})O_2$ by ZrO_2 Coating for Lithium Ion Batteries. *J. Appl. Electrochem.* **2017**, *47* (5), 565–572.

(31) Sun, Y.-K.; Chen, Z.; Noh, H.-J.; Lee, D.-J.; Jung, H.-G.; Ren, Y.; Wang, S.; Yoon, C. S.; Myung, S.-T.; Amine, K. Nanostructured High-Energy Cathode Materials for Advanced Lithium Batteries. *Nat. Mater.* **2012**, *11* (11), 942–947.

(32) Toby, B. H. EXPGUI, a Graphical User Interface for GSAS. *J. Appl. Crystallogr.* **2001**, *34* (2), 210–213.

(33) Ravel, B.; Newville, M. ATHENA, ARTEMIS, HEPHAESTUS: Data Analysis for X-Ray Absorption Spectroscopy Using IFEFFIT. *J. Synchrotron Rad* **2005**, *12*, 537–541.

(34) Weng, T.-C.; Waldo, G. S.; Penner-Hahn, J. E. A Method for Normalization of X-Ray Absorption Spectra. *J. Synchrotron Radiat.* **2005**, *12* (4), 506–510.

(35) Liu, Y.; Andrews, J. C.; Meirer, F.; Mehta, A.; Gil, S. C.; Sciau, P.; Mester, Z.; Pianetta, P. Applications of Hard X-Ray Full-Field Transmission X-Ray Microscopy at SSRL. *AIP Conf. Proc.* **2011**, *1365*, 305.

(36) Yoon, W.-S.; Chung, K. Y.; McBreen, J.; Yang, X.-Q. A Comparative Study on Structural Changes of $LiCo_{1/3}Ni_{1/3}Mn_{1/3}O_2$ and $LiNi_{0.8}Co_{0.15}Al_{0.05}O_2$ during First Charge Using in Situ XRD. *Electrochem. commun.* **2006**, *8* (8), 1257–1262.

(37) Choi, J.; Alvarez, E.; Arunkumar, T. A.; Manthiram, A. Proton Insertion into Oxide Cathodes during Chemical Delithiation. *Electrochem. Solid-State Lett.* **2006**, *9* (5), A241.

(38) Yang, X. .; Sun, X.; McBreen, J. New Findings on the Phase Transitions in $Li_{1-x}NiO_2$: In Situ Synchrotron X-Ray Diffraction Studies. *Electrochem. commun.* **1999**, *1* (6), 227–232.

(39) Li, J.; Shunmugasundaram, R.; Doig, R.; Dahn, J. R. In Situ X-Ray Diffraction Study of Layered Li–Ni–Mn–Co Oxides: Effect of Particle Size and Structural Stability of Core–Shell Materials. *Chem. Mater.* **2016**, *28* (1), 162–171.

(40) Van Oversteeg, C. H. M.; Doan, H. Q.; De Groot, F. M. F.; Cuk, T. In Situ X-Ray

Absorption Spectroscopy of Transition Metal Based Water Oxidation Catalysts. *Chemical Society Reviews*. Royal Society of Chemistry January 1, 2017, pp 102–125.

(41) De Groot, F.; Vankó, G.; Glatzel, P. The 1s X-Ray Absorption Pre-Edge Structures in Transition Metal Oxides. *J. Phys. Condens. Matter* **2009**, *21* (10), 104207–104214.

(42) Yamamoto, T. Assignment of Pre-Edge Peaks in K-Edge x-Ray Absorption Spectra of 3d Transition Metal Compounds: Electric Dipole or Quadrupole? *X-Ray Spectrometry*. John Wiley and Sons Ltd 2008, pp 572–584.

(43) Deb, A.; Bergmann, U.; Cramer, S. P.; Cairns, E. J. *In Situ* x-Ray Absorption Spectroscopic Study of the $Li[Ni_{1/3}Co_{1/3}Mn_{1/3}]O_2$ Cathode Material. *J. Appl. Phys.* **2005**, *97* (11), 113523.

(44) Henderson, G. S.; De Groot, F. M. F.; Moulton, B. J. A. X-Ray Absorption Near-Edge Structure (XANES) Spectroscopy. *Spectrosc. Methods Mineral. Geol.* **2014**, *78*, 75–138.

(45) Nakai, I. In Situ Transmission X-Ray Absorption Fine Structure Analysis of the Li Deintercalation Process in $Li(Ni_{0.5}Co_{0.5})O_2$. *Electrochem. Solid-State Lett.* **1999**, *1* (6), 259.

(46) Balasubramanian, M.; McBreen, J.; Davidson, I. J.; Whitfield, P. S.; Kargina, I. In Situ X-Ray Absorption Study of a Layered Manganese-Chromium Oxide-Based Cathode Material. *J. Electrochem. Soc.* **2002**, *149* (2), A176.

(47) Yoon, W.-S.; Paik, Y.; Yang, X.-Q.; Balasubramanian, M.; McBreen, J.; Grey, C. P. Investigation of the Local Structure of the $LiNi_{0.5}Mn_{0.5}O_2$ Cathode Material

during Electrochemical Cycling by X-Ray Absorption and NMR Spectroscopy. *Electrochem. Solid-State Lett.* **2002**, *5* (11), A263.

(48) Manceau, A.; Gorshkov, A. I.; Drits, V. A. Structural Chemistry of Mn, Fe, Co, and Ni in Manganese Hydrous Oxides: Part I. Information from XANES Spectroscopy. *Am. Mineral.* **1992**, *77* (11–12), 1133–1143.

(49) Horne, C. R.; Bergmann, U.; Grush, M. M.; Perera, R. C. C.; Ederer, D. L.; Callcott, T. A.; Cairns, E. J.; Cramer, S. P. Electronic Structure of Chemically-Prepared $Li_xMn_2O_4$ Determined by Mn X-Ray Absorption and Emission Spectroscopies . *J. Phys. Chem. B* **2002**, *104* (41), 9587–9596.

(50) Tian, C.; Xu, Y.; Nordlund, D.; Lin, F.; Liu, J.; Sun, Z.; Liu, Y.; Doeff, M. Charge Heterogeneity and Surface Chemistry in Polycrystalline Cathode Materials. *Joule* **2018**, *2* (3), 464–477.

(51) Lin, F.; Liu, Y.; Yu, X.; Cheng, L.; Singer, A.; Shpyrko, O. G.; Xin, H. L.; Tamura, N.; Tian, C.; Weng, T.-C.; Yang, X.-Q.; Meng, Y. S.; Nordlund, D.; Yang, W.; Doeff, M. M. Synchrotron X-Ray Analytical Techniques for Studying Materials Electrochemistry in Rechargeable Batteries. *Chem. Rev.* **2017**, *117* (21), 13123–13186.

(52) Tian, C.; Lin, F.; Doeff, M. M. Electrochemical Characteristics of Layered Transition Metal Oxide Cathode Materials for Lithium Ion Batteries: Surface, Bulk Behavior, and Thermal Properties. *Acc. Chem. Res.* **2018**, *51* (1), 89–96.

(53) Yogi, C.; Takamatsu, D.; Yamanaka, K.; Arai, H.; Uchimoto, Y.; Kojima, K.; Watanabe, I.; Ohta, T.; Ogumi, Z. Soft X-Ray Absorption Spectroscopic Studies with Different Probing Depths: Effect of an Electrolyte Additive on Electrode

Surfaces. *J. Power Sources* **2014**, *248*, 994–999.

(54) Lin, F.; Nordlund, D.; Markus, I. M.; Weng, T.-C.; Xin, H. L.; Doeff, M. M. Profiling the Nanoscale Gradient in Stoichiometric Layered Cathode Particles for Lithium-Ion Batteries. *Energy Environ. Sci.* **2014**, *7* (9), 3077.

(55) Steiner, J. D.; Mu, L.; Walsh, J.; Rahman, M. M.; Zydlewski, B.; Michel, F. M.; Xin, H. L.; Nordlund, D.; Lin, F. Accelerated Evolution of Surface Chemistry Determined by Temperature and Cycling History in Nickel-Rich Layered Cathode Materials. *ACS Appl. Mater. Interfaces* **2018**, *10* (28), 23842–23850.

(56) Jung, R.; Metzger, M.; Maglia, F.; Stinner, C.; Gasteiger, H. A. Oxygen Release and Its Effect on the Cycling Stability of $LiNi_xMn_yCo_zO_2$ (NMC) Cathode Materials for Li-Ion Batteries . *J. Electrochem. Soc.* **2017**, *164* (7), A1361–A1377.

(57) Mu, L.; Yuan, Q.; Tian, C.; Wei, C.; Zhang, K.; Liu, J.; Pianetta, P.; Doeff, M. M.; Liu, Y.; Lin, F. Propagation Topography of Redox Phase Transformations in Heterogeneous Layered Oxide Cathode Materials. *Nat. Commun.* **2018**, *9* (1), 2810.

(58) Bergmann, U.; Glatzel, P.; Cramer, S. P. Bulk-Sensitive XAS Characterization of Light Elements: From X-Ray Raman Scattering to X-Ray Raman Spectroscopy. *Microchem. J.* **2002**, *71* (2–3), 221–230.

(59) Sokaras, D.; Nordlund, D.; Weng, T. C.; Mori, R. A.; Velikov, P.; Wenger, D.; Garachtchenko, A.; George, M.; Borzenets, V.; Johnson, B.; Qian, Q.; Rabedeau, T.; Bergmann, U. A High Resolution and Large Solid Angle X-Ray Raman Spectroscopy End-Station at the Stanford Synchrotron Radiation Lightsource. *Review of Scientific Instruments*. April 2012, p 043112.

(60) Li, Y.; El Gabaly, F.; Ferguson, T. R.; Smith, R. B.; Bartelt, N. C.; Sugar, J. D.; Fenton, K. R.; Cogswell, D. A.; Kilcoyne, A. L. D.; Tyliszczak, T.; Bazant, M. Z.; Chueh, W. C. Current-Induced Transition from Particle-by-Particle to Concurrent Intercalation in Phase-Separating Battery Electrodes. *Nat. Mater.* **2014**, *13* (12), 1149–1156.

(61) Kuppan, S.; Xu, Y.; Liu, Y.; Chen, G. Phase Transformation Mechanism in Lithium Manganese Nickel Oxide Revealed by Single-Crystal Hard X-Ray Microscopy. *Nat. Commun.* **2017**, *8*, 14309.

(62) Xu, Y.; Hu, E.; Zhang, K.; Wang, X.; Borzenets, V.; Sun, Z.; Pianetta, P.; Yu, X.; Liu, Y.; Yang, X.-Q.; Li, H. In Situ Visualization of State-of-Charge Heterogeneity within a $LiCoO_2$ Particle That Evolves upon Cycling at Different Rates. *ACS Energy Lett.* **2017**, *2* (5), 1240–1245.

(63) Mao, Y.; Wang, X.; Xia, S.; Zhang, K.; Wei, C.; Bak, S.; Shadike, Z.; Liu, X.; Yang, Y.; Xu, R.; Pianetta, P.; Ermon, S.; Stavitski, E.; Zhao, K.; Xu, Z.; Lin, F.; Yang, X. Q.; Hu, E.; Liu, Y. High-Voltage Charging-Induced Strain, Heterogeneity, and Micro-Cracks in Secondary Particles of a Nickel-Rich Layered Cathode Material. *Adv. Funct. Mater.* **2019**, *29* (18), 1900247.

(64) Xia, S.; Mu, L.; Xu, Z.; Wang, J.; Wei, C.; Liu, L.; Pianetta, P.; Zhao, K.; Yu, X.; Lin, F.; Liu, Y. Chemomechanical Interplay of Layered Cathode Materials Undergoing Fast Charging in Lithium Batteries. *Nano Energy* **2018**, *53*, 753–762.

(65) Li, S.; Lee, S.-J.; Wang, X.; Yang, W.; Huang, H.; Swetz, D. S.; Doriese, W. B.; O'Neil, G. C.; Ullom, J. N.; Titus, C. J.; Irwin, K. D.; Lee, H.-K.; Nordlund, D.; Pianetta, P.; Yu, C.; Qiu, J.; Yu, X.; Yang, X.-Q.; Hu, E.; Lee, J.-S.; Liu, Y.

Surface-to-Bulk Redox Coupling through Thermally Driven Li Redistribution in Li- and Mn-Rich Layered Cathode Materials. *J. Am. Chem. Soc.* **2019**, *141* (30), 12079–12086.

(66) Zhengrui, X.; Muhammad Mominur, R.; Linqin, M.; Yijin, L.; Feng, L. Chemomechanical Behaviors of Layered Cathode Materials in Alkali Metal Ion Batteries. *J. Mater. Chem. A* **2018**, *6*, 21859–21884.

(67) Li, Y. A Review of Recent Research on Nonequilibrium Solid Solution Behavior in Li_XFePO_4. *Solid State Ionics* **2018**, *323*, 142–150.

(68) Patoux, S.; Doeff, M. M. Direct Synthesis of $LiNi_{1/3}Co_{1/3}Mn_{1/3}O_2$ from Nitrate Precursors. Electrochem. Commun. 2004, 6, 767–772.

(69) Lin, R.; Hu, E.; Liu, M.; Wang, Y.; Cheng, H.; Wu, J.; Zheng, J.-C.; Wu, Q.; Bak, S.; Tong, X.; Zhang, R.; Yang, W.; Persson, K. A.; Yu, X.; Yang, X.-Q.; Xin, H.L. Anomalous Metal Segregation in Lithium-Rich Material Provides Design Rules for Stable Cathode in Lithium-Ion Battery. Nat. Commun. 2019, 10, 1650.

For Table of Contents Only